SUPPLEMENTARY MATERIAL.

Equations.

Equations from the CPCD model were taken from reference 14. Some terms were added to account for processes that we believe are crucial. In eq. 1 a term for electron-capture process in gas phase is added. In eq. 5 an extra energy term for the internal vibrational conversion (IVR) occurring after excitation of S_1 to S_n was added. Eq. 6 is written for thermal ionization S_n. Eq. 7, 8, 9, 10, 11 and 12 are new. Eq. 13 is the correction function described in ref. 14 and it is written here for clarification. Values of different constant used in this model where taken from ref. 14 (Tab. 1) or are included in Tab. 1 of the paper.

$$\frac{d[S_0]}{dt} = -I(t)\sigma_{01}(\lambda)[S_0] + \frac{[S_1]}{C\boldsymbol{\tau_1}(\overline{\boldsymbol{T}}_{\boldsymbol{T}})} + I(t)(\sigma_{01}(\lambda)/5)[S_1] + \boldsymbol{Corr}(\overline{\boldsymbol{T}}_{\boldsymbol{T}})Dk_{11}[S_1]^2 + \boldsymbol{Corr}(\overline{\boldsymbol{T}}_{\boldsymbol{T}})Dk_{1n}[S_1][S_n] + \boldsymbol{Corr}(\overline{\boldsymbol{T}}_{\boldsymbol{T}})k_{I0}[M^+] - \boldsymbol{\sigma_{ECI}}\overline{\boldsymbol{v}}_{\boldsymbol{e}}\frac{\boldsymbol{n_0}}{\boldsymbol{Vn}}\boldsymbol{NLPE(t)}[\boldsymbol{S_0}]\boldsymbol{Exp}[-\boldsymbol{EA}/\boldsymbol{K_BT_V}] \quad (1)$$

$$\frac{d[S_1]}{dt} = I(t)\sigma_{01}(\lambda)[S_0] - \frac{[S_1]}{C\boldsymbol{\tau_1}(\overline{\boldsymbol{T}}_{\boldsymbol{T}})} - I(t)(\sigma_{01}(\lambda)/5)[S_1] - I(t)(\sigma_{1n}(\lambda)/5)[S_1] + \boldsymbol{Corr}(\overline{\boldsymbol{T}}_{\boldsymbol{T}})k_{n1}[S_n] - \boldsymbol{Corr}(\overline{\boldsymbol{T}}_{\boldsymbol{T}})2Dk_{11}[S_1]^2 - \boldsymbol{Corr}(\overline{\boldsymbol{T}}_{\boldsymbol{T}})Dk_{1n}[S_1][S_n] \quad (2)$$

$$\frac{d[S_n]}{dt} = I(t)\sigma_{01}(\lambda)[S_1] - \boldsymbol{Corr}(\overline{\boldsymbol{T}}_{\boldsymbol{T}})k_{n1}[S_n] - k_{therm}[S_n] + \boldsymbol{Corr}(\overline{\boldsymbol{T}}_{\boldsymbol{T}})Dk_{11}[S_1]^2 - \boldsymbol{Corr}(\overline{\boldsymbol{T}}_{\boldsymbol{T}})Dk_{1n}[S_1][S_n] \quad (3)$$

$$\frac{d[M^+]}{dt} = +k_{therm}[S_n] + \boldsymbol{Corr}(\overline{\boldsymbol{T}}_{\boldsymbol{T}})Dk_{1n}[S_1][S_n] - \boldsymbol{Corr}(\overline{\boldsymbol{T}}_{\boldsymbol{T}})Dk_{I0}[M^+] \quad (4)$$

$$\frac{d[\varepsilon_V]}{dt} = I(t)\sigma_{01}(\lambda)[S_0]\{h\upsilon - \varepsilon(S_1)\} + \boldsymbol{I(t)\sigma_{n1}(\lambda)}[\boldsymbol{S_1}]\{\boldsymbol{h\upsilon} - \boldsymbol{\varepsilon(S_n)}\} + \frac{[S_1]}{C\boldsymbol{\tau_1}(\overline{\boldsymbol{T}}_{\boldsymbol{T}})}\{\varepsilon(S_1)(1 - \boldsymbol{C\phi(S_1)}(\overline{\boldsymbol{T}}_{\boldsymbol{T}}))\} + \boldsymbol{Corr}(\overline{\boldsymbol{T}}_{\boldsymbol{T}})k_{n1}\{\varepsilon(S_n) - \varepsilon(S_1)\} + \boldsymbol{Corr}(\overline{\boldsymbol{T}}_{\boldsymbol{T}})Dk_{1n}[S_1][S_n]\{\varepsilon(S_1) + \varepsilon(S_n) - IP\} + \boldsymbol{Corr}(\overline{\boldsymbol{T}}_{\boldsymbol{T}})Dk_{I0}[M^+]IP \quad (5)$$

$$k_{therm} = 9 * 10^{15}Exp[(\varepsilon(S_n) - IP)/K_BT_V] \quad (6)$$

$$\frac{\boldsymbol{d[M^-]}}{\boldsymbol{dt}} = \boldsymbol{\sigma_{ECI}}\overline{\boldsymbol{v}}_{\boldsymbol{e}}\frac{\boldsymbol{n_0}}{\boldsymbol{Vn}}\boldsymbol{NLPE(t)}[\boldsymbol{S_0}]\boldsymbol{Exp}[-\boldsymbol{EA}/\boldsymbol{k_BT_V}] - \frac{\boldsymbol{1}}{\boldsymbol{\tau_{M^-}}}[\boldsymbol{M^-}] - \boldsymbol{k_{TSH}}[\boldsymbol{M^-}] - \boldsymbol{k_{TSH2}}[\boldsymbol{M^-}] \quad (7)$$

$$\frac{\boldsymbol{d[M-H]^-}}{\boldsymbol{dt}} = \boldsymbol{k_{TSH}}[\boldsymbol{M^-}] \quad (8)$$

$$\frac{\boldsymbol{d[M-H_2]^-}}{\boldsymbol{dt}} = \boldsymbol{k_{TSH2}}[\boldsymbol{M^-}] \quad (9)$$

$$\boldsymbol{m_1C_V}\frac{\boldsymbol{dT_1}}{\boldsymbol{dt}} - \boldsymbol{C_VT_1}\frac{\boldsymbol{dm_1}}{\boldsymbol{dt}} = \boldsymbol{F_1S_1I(t)} - \frac{\boldsymbol{K_{DHB}S_1(T_1-T_2)}}{\boldsymbol{l_1}} - \boldsymbol{S_1\epsilon\sigma}(\boldsymbol{T_1^4} - \boldsymbol{T_0^4}) - \frac{\boldsymbol{\Delta H_{Sub}}}{\boldsymbol{W_{DHB}}}\frac{\boldsymbol{dm_1}}{\boldsymbol{dt}} \quad (10)$$

$$\boldsymbol{m_2C_V}\frac{\boldsymbol{dT_2}}{\boldsymbol{dt}} - \boldsymbol{C_VT_2}\frac{\boldsymbol{dm_2}}{\boldsymbol{dt}} = \boldsymbol{F_1S_2I(t)} - \frac{\boldsymbol{K_{DHB}S_2(T_2-T_3)}}{\boldsymbol{l_2}} + \frac{\boldsymbol{K_{DHB}S_1(T_1-T_2)}}{\boldsymbol{l_1}} - \boldsymbol{S_2\epsilon\sigma}(\boldsymbol{T_2^4} - \boldsymbol{T_0^4}) - \frac{\boldsymbol{\Delta H_{Sub}}}{\boldsymbol{W_{DHB}}}\frac{\boldsymbol{dm_2}}{\boldsymbol{dt}} \quad (11)$$

$$\boldsymbol{m_3C_V}\frac{\boldsymbol{dT_3}}{\boldsymbol{dt}} - \boldsymbol{C_VT_3}\frac{\boldsymbol{dm_3}}{\boldsymbol{dt}} = \boldsymbol{F_1S_3I(t)} - \frac{\boldsymbol{K_{DHB}S_3(T_3-T_0)}}{\boldsymbol{l_3}} + \frac{\boldsymbol{K_{DHB}S_1(T_2-T_3)}}{\boldsymbol{l_1}} - \boldsymbol{S_3\epsilon\sigma}(\boldsymbol{T_3^4} - \boldsymbol{T_0^4}) - \frac{\boldsymbol{\Delta H_{Sub}}}{\boldsymbol{W_{DHB}}}\frac{\boldsymbol{dm_3}}{\boldsymbol{dt}} \quad (12)$$

$$\boldsymbol{Corr}(\overline{\boldsymbol{T}}_{\boldsymbol{T}}) = \begin{cases} \boldsymbol{0}, & \boldsymbol{if\ T < T_S} \\ \boldsymbol{p/p_0} = \left(\boldsymbol{1} + \frac{\boldsymbol{\gamma-1}}{\boldsymbol{2}}\boldsymbol{Ma^2}\right)^{-\boldsymbol{\gamma}/(\boldsymbol{\gamma-1})}, & \boldsymbol{if\ T \geq T_S} \end{cases} \quad (13)$$

$$C\tau_1(\overline{T}_T) = \begin{cases} 10^{-9} & , \ if \ T < T_S \\ 3 \cdot 10^{-9} & , \ if \ T \geq T_S \end{cases} \quad (14)$$

$$C\phi(S_1)(\overline{T}_T) = \begin{cases} 1 & , \ if \ T < T_S \\ 1/3 & , \ if \ T \geq T_S \end{cases} \quad (15)$$

Temperature calculation.

Conductivity data was taken from ref. 67. In fig. 1 a plot of the conductivity value as a function of T is presented. The variation follows a nearly linear trend ($0.27 - 2.3 \times 10^{-4}T + 9.2 \times 10^{-8}T^2$) over the range taken from ref. 67. (480-780 K). Extrapolated values from the fit were taken for values of temperatures between 299-479 K and 781-above K.

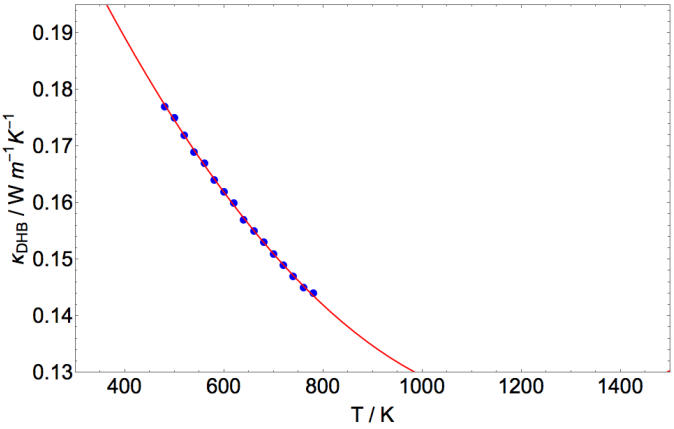

Fig. 1. Variation oft he DHB heat conductivity as a function of the T. Data of κ_{DHB} for a temperature range between 480 and 780 K was taken from ref 67. The blue dots represent the values of κ_{DHB} meanwhile the red line is a first order polynomial.

An exemplary calculation for variation of temperature as a function of time in each layer is drawn in fig. 2. It can be seen that temperature in second layer does not overcome at any time the T_{Sub}, which is marked by a horizontal brown line. Several authors have described theoretically the T of the MALDI process in a way that it remains constant as a function of time after laser pulse is finished. However, measurements made (ref. 89) showed that temperature rises up to a maximum, which is delayed from the laser maximum, and then decays fast. Here we have obtained a similar behavior, as shown in fig. 2, with the exception of the fast decay that Koubenakis et al. have reported (ref. 89). This feature is the most probably occurring due to the sudden change of heat conductivity at high temperatures.

With our calculation it is clear that the molecules and ions will have a distribution of energies and in consequence of speed. We have considered an average temperature ($\overline{T}$) equal to the maximum, which is used to defined a stream-initial temperature u_0.

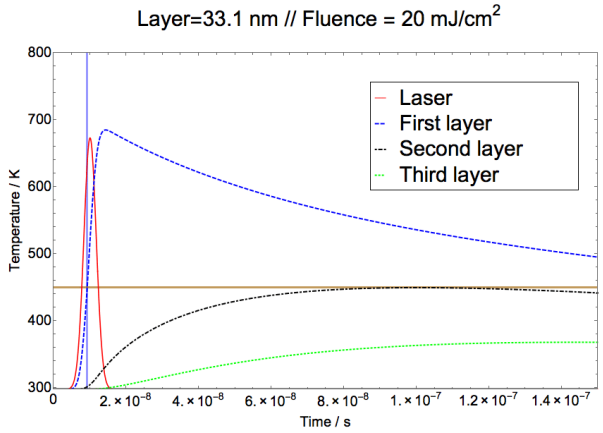

Fig. 2. Temperature variation as a function of time for three layers of same thickness (3.35 nm). Fluence was 20 mJ/cm^2. Irradiance of laser is shown over time. Temperature of second layer does not surpass at any time the sublimation temperature. Maximum temperature of layer one is reached a ns after the maximum of laser pulse. The violet vertical line shows the time at which T_{Sub} is reached (0.9 ns). Variation of parameter $\Delta\beta$ is shown in fig. 3. The trend is linear from 4.5 to 100 mJ/cm^2.

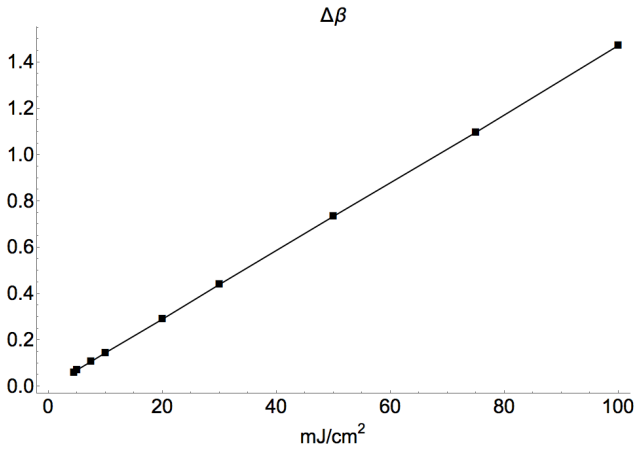

Fig. 3. Variation $\Delta\beta$ parameter as a function of fluence.

Speed: Maxwell-Boltzmann distribution.

The average translational temperature is calculated according the three-layer model. The maximum is reached 1 ns later than the maximum of the laser power. This temperature is used to calculate a stream velocity according to,

$$u_0 = (2K_B\bar{T}_T/m)^{0.5} \tag{13}$$

with m the mass of single DHB molecule, K_B the Boltzmann constant and $\bar{T}_T$ the average temperature. Thus, a MB distribution can be calculated according eq. 2 written in paper. The result is shown in fig 3, where the most probable speed is marked with a vertical grey line.

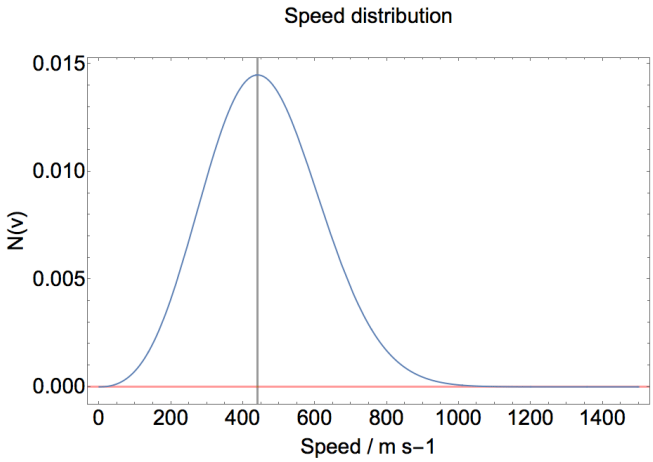

Fig. 4. MB distribution with the most probable (v_p, grey).

In order to check how distinct the yields of different species as a function of the ion speed is, we have solved parametrically the system of equations. The chosen parameter was the speed of the ions which is included in the Mach number $M(\bar{T}_T) = speed/(\gamma(\bar{T}_T)R\bar{T}_T)/MW_{DHB})^{0.5}$ which is the quotient between the ion speed and the ideal gas speed of sound. The M number is function of the T by definition, which means that if temperature increase over T_{Sub}, M will increase . Therefore, its variation has to be calculated over time. It is included in equations 1 and 8 of the paper. Equation 1 is used to correct the pooling and ion-recombination constants according CPCD model. Equation 8 includes a volume correction through a supersonic density ratio. Fig. 4 shows the behavior of species M^+, M^-, $[M\text{-}H]^-$ and $[M\text{-}H_2]^-$ for a fluence of 20 mJ/cm^2. Fig. 5 shows the same, but for 100 mJ/cm^2.

Distribution of speed of electrons.

Here, a distribution of energies for electron both from stainless steel and gold surfaces is shown. The emission profiles were taken from ref. 17 and adjusted to a Cauchy-Lorentz distribution. Maximum energies are 0.55 eV and 1.0 eV for gold and stainless steel, respectively. These values corresponds to the maximum energy according to $KE_{max} = h\nu - \phi$. Here, we have taken the energy corresponding to the maximum of the distribution.

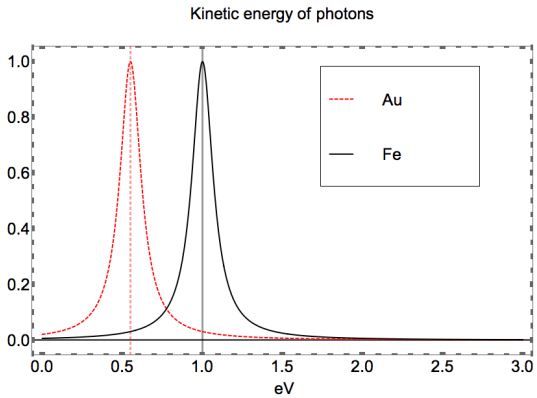

Figure 5. Energy distribution of photoelectrons emitted from the bulk metal (stainless steel and gold) as in ref. 17.

Variaton of autoionzation and RRKM constants as a function of time.

The constants for both unimolecular dissociation processes (H and H_2 loss) and autoionzation are depicted versus vibrational energy in fig. 6, 7, 8 and 9.

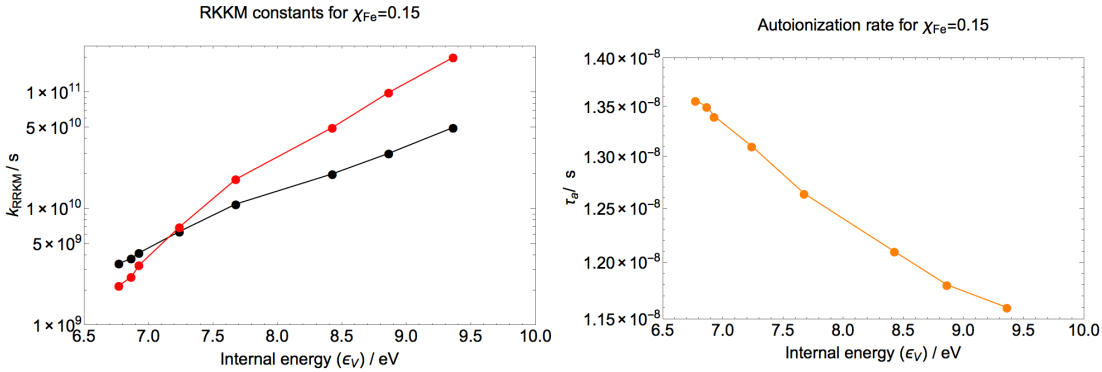

Fig. 6. Left: RRKM constant for unimolecular dissociation channels yielding $[DHB\text{-}H]^-$ (black) and $[DHB\text{-}H_2]^-$ (red) loss. Right: autoionization lifetime as a function of the internal energy (ε_V) for χ_{Fe} = 0.15.

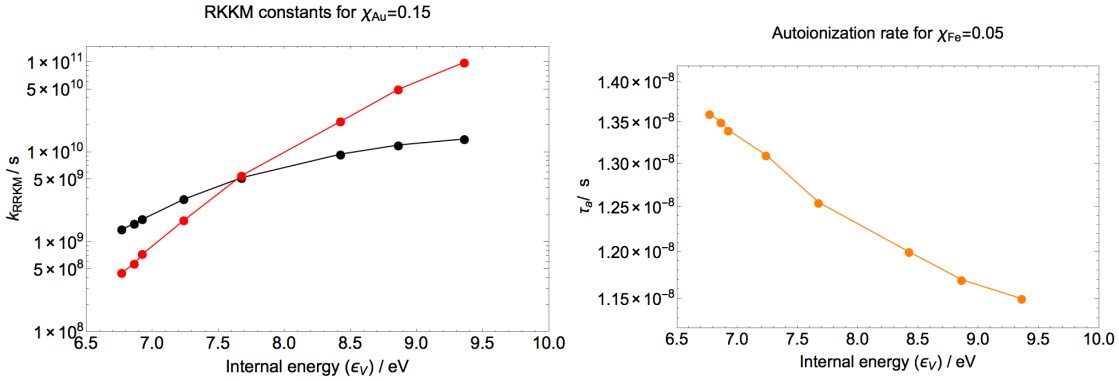

Fig. 7. Left: RRKM constant for unimolecular dissociation channels yielding $[DHB\text{-}H]^-$ (black) and $[DHB\text{-}H_2]^-$ (red) loss. Right: autoionization lifetime as a function of the internal energy (ε_V) for χ_{Fe} = 0.05.

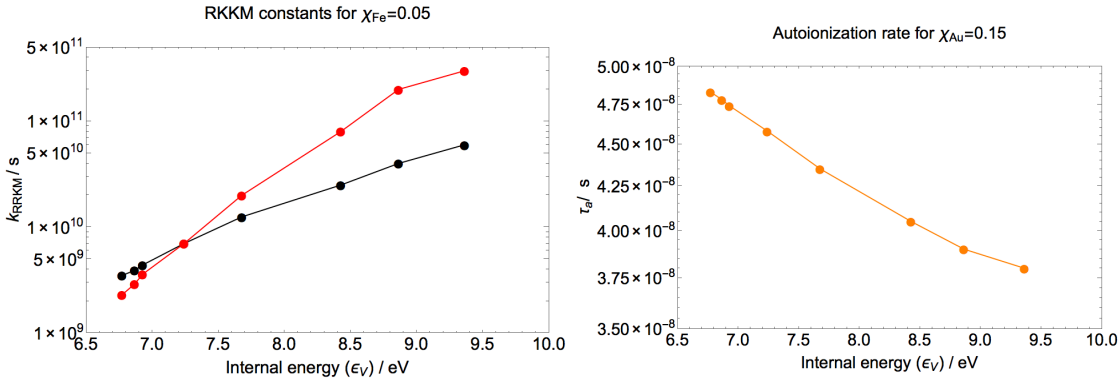

Fig. 8. Left: RRKM constant for unimolecular dissociation channels yielding $[DHB\text{-}H]^-$ (black) and $[DHB\text{-}H_2]^-$ (red) loss. Right: autoionization lifetime as a function of the internal energy (ε_V) for χ_{Au} = 0.15.

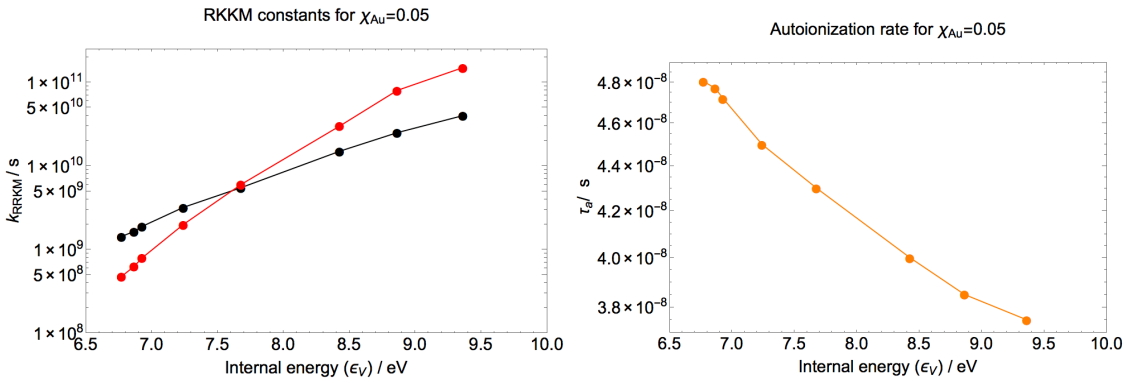

Fig. 9. Left: RRKM constant for unimolecular dissociation channels yielding $[DHB\text{-}H]^-$ (black) and $[DHB\text{-}H_2]^-$ (red) loss. Right: autoionization lifetime as a function of the internal energy (ε_V) for χ_{Au} = 0.05.

Mass spectra and negative ion yield as a function of fluence.

Exemplary mass spectra of M^-, $[M\text{-}H]^-$ and $[M\text{-}H_2]^-$ are shown in fig. 10, 11, 12 and 13 for different fluences, metals and DHB coverage. Fig. 14, 15 and 12 show the ion yield of M^-, $[M\text{-}H]^-$ and $[M\text{-}H_2]^-$ as a function of fluence for two metals and different coverages. These three graphs are complementary to the fig. 13 in manuscript.

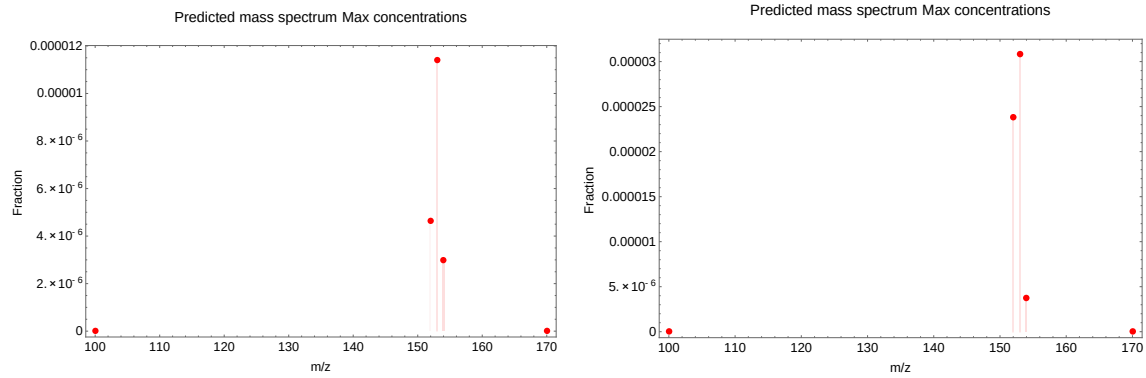

Fig. 10. Maximum negative ion yield predicted mass spectrum for 20 mJ/cm^2 and χ_{DHB} = 0.85 in Au (left) and same conditions for Fe (right).

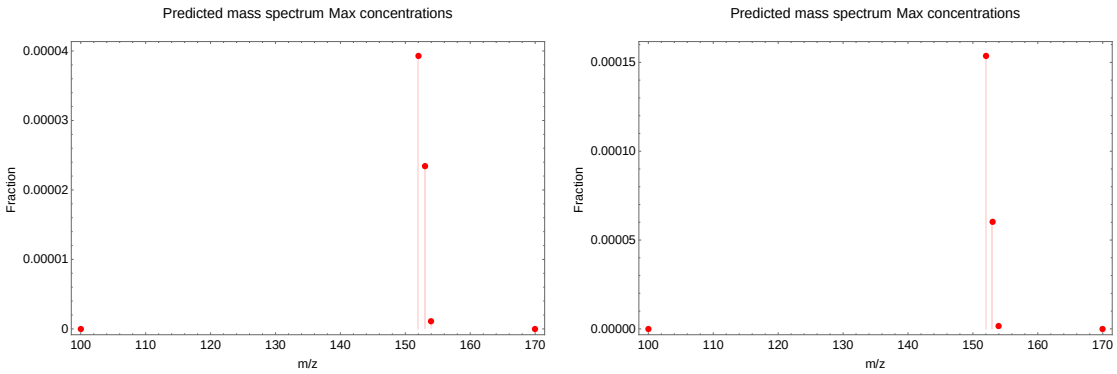

Fig. 11. Maximum negative ion yield predicted mass spectrum for 100 mJ/cm^2 and χ_{DHB} = 0.85 in Au (left) and same conditions for Fe (right).

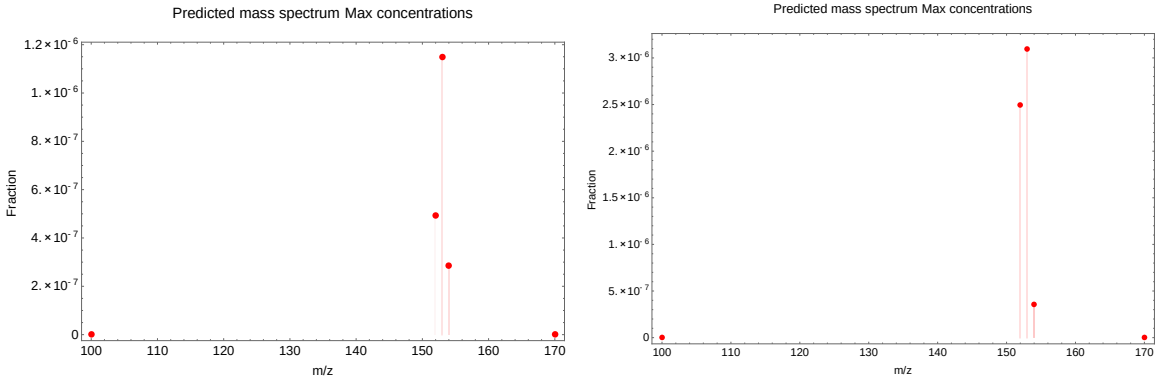

Fig. 12. Maximum negative ion yield predicted mass spectrum for 20 mJ/cm^2 and χ_{DHB} = 0.95 in Au (left) and same conditions for Fe (right).

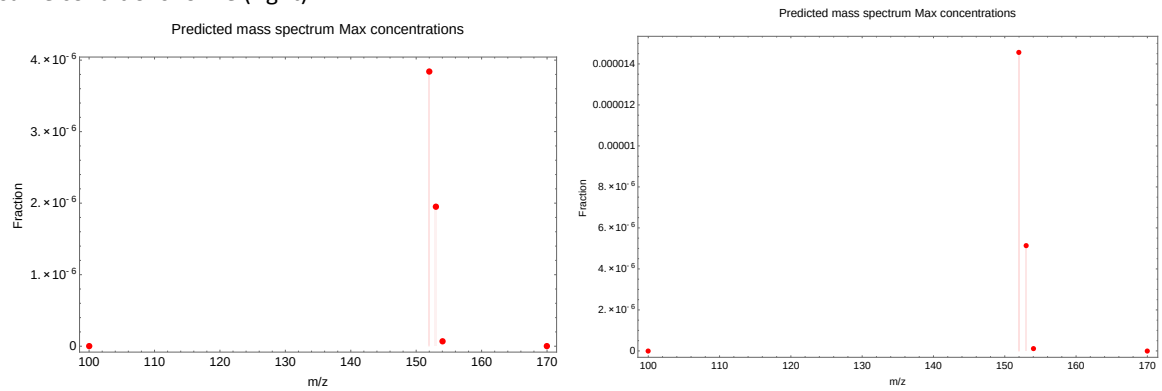

Fig. 13. Maximum negative ion yield predicted mass spectrum for 100 mJ/cm^2 and χ_{DHB} = 0.95 in Au (left) and same conditions for Fe (right).

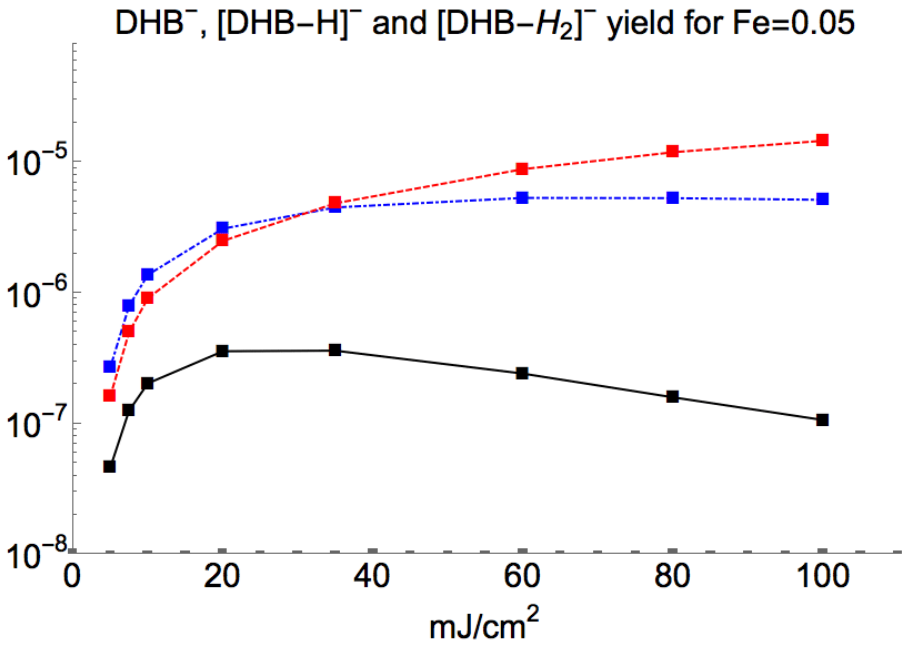

Fig. 14. Ion yield for the three negative species as a function of fluence for Fe and χ_{DHB} = 0.95. M^- (black), $[M\text{-}H]^-$ (blue dashed) and $[M\text{-}H_2]^-$ (red dotted).

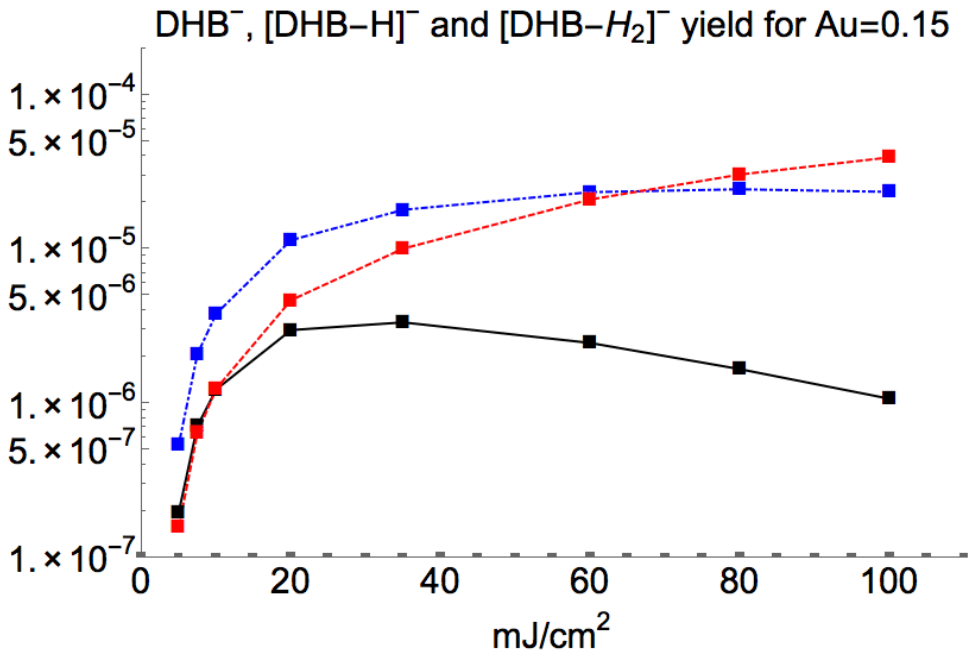

Fig. 15. Ion yield for the three negative species as a function of fluence for Au and χ_{DHB} = 0.85. M^- (black), $[M\text{-}H]^-$ (blue dashed) and $[M\text{-}H_2]^-$ (red dotted).

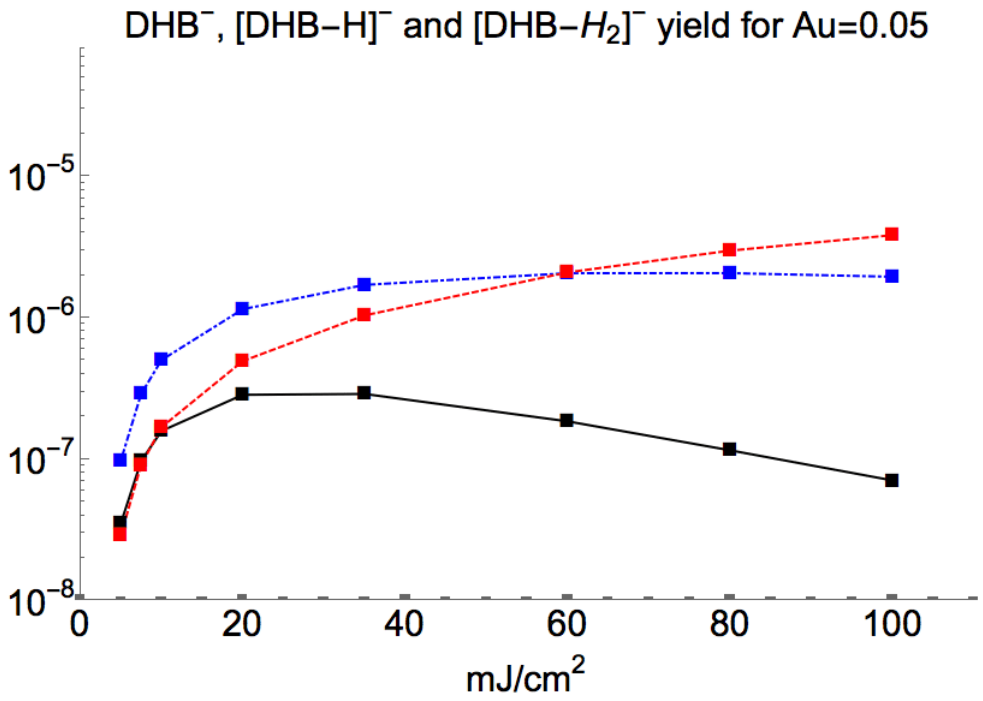

Fig. 16. Ion yield for the three negative species as a function of fluence for Au and χ_{DHB} = 0.95. M^- (black), $[M\text{-}H]^-$ (blue dashed) and $[M\text{-}H_2]^-$ (red dotted).